RADIO SCIENCE, VOL. 44, RS1008, doi:10.1029/2008RS003897, 2009

Sensitivity analysis and performance estimation of refractivity from clutter techniques

Caglar Yardim,[1] Peter Gerstoft,[1] and William S. Hodgkiss[1]

Received 9 May 2008; revised 30 October 2008; accepted 11 December 2008; published 17 February 2009.

[1] Refractivity from clutter (RFC) refers to techniques that estimate the atmospheric refractivity profile from radar clutter returns. A RFC algorithm works by finding the environment whose simulated clutter pattern matches the radar measured one. This paper introduces a procedure to compute RFC estimator performance. It addresses the major factors such as the radar parameters, the sea surface characteristics, and the environment (region, time of the day, season) that affect the estimator performance and formalizes an error metric combining all of these. This is important for applications such as calculating the optimal radar parameters, selecting the best RFC inversion algorithm under a set of conditions, and creating a regional performance map of a RFC system. The performance metric is used to compute the RFC performance of a non-Bayesian evaporation duct estimator. A Bayesian estimator that incorporates meteorological statistics in the inversion is introduced and compared to the non-Bayesian estimator. The performance metric is used to determine the optimal radar parameters of the evaporation duct estimator for six scenarios. An evaporation duct inversion performance map for a S band radar is created for the larger Mediterranean/Arabian Sea region.

Citation: Yardim, C., P. Gerstoft, and W. S. Hodgkiss (2009), Sensitivity analysis and performance estimation of refractivity from clutter techniques, *Radio Sci.*, *44*, RS1008, doi:10.1029/2008RS003897.

1. Introduction

[2] Electromagnetic ducts are formed by small variations in the index of refraction due to sharp inversions in the vertical atmospheric temperature and humidity profiles. Evaporation from ocean surface, creation of marine boundary layers, and interactions between warm and dry land-based air systems with humid conditions above the sea surface are some of the meteorological mechanisms for duct formation. Hence, atmospheric ducting is frequently encountered in open oceans and coastal zones of tropical and subtropical regions around the world.

[3] Many of the lower atmospheric maritime radar systems have to operate under these ducting conditions. Electromagnetic ducts result in nonstandard electromagnetic propagation which fundamentally can change the performance of a system that is designed to operate under standard atmospheric conditions with a typical slope of 0.118 M-units/m. These include a change in the maximum operational radar range, creation of radar holes where the radar effectively is blind, target altitude errors and large sea surface clutter due to the increased interaction between the electromagnetic signal trapped within the duct and the sea surface [*Skolnik*, 2001].

[4] Conventionally atmospheric refractivity is measured using radiosondes and rocketsondes, microwave refractometers, and predicted by meteorological models such as the Coupled Ocean/Atmospheric Mesoscale Prediction System (COAMPS) [*Rowland and Babin*, 1987; *Thews*, 1990; *Hodur*, 1996]. There also are other techniques that can predict refractivity using lidar [*Willitsford and Philbrick*, 2005] and GPS [*Lowry et al.*, 2002] measurements. However, the radar itself can also be used to estimate the refractivity. These techniques are termed refractivity from clutter (RFC) techniques and they estimate the modified refractivity profile (M profile) by taking advantage of the changes in radar clutter return due to atmospheric refraction [*Rogers et al.*, 2000; *Gerstoft et al.*, 2003, 2004; *Barrios*, 2004; *Rogers et al.*, 2005; *Yardim et al.*, 2006; *Vasudevan et al.*, 2007;

[1]Marine Physical Laboratory, Scripps Institution of Oceanography, University of California, San Diego, La Jolla, California, USA.

0048-6604/09/2008RS003897$11.00

Yardim et al., 2007, 2008]. Detailed discussions about these different RFC algorithms can be found in the works of *Vasudevan et al.* [2007] and *Yardim et al.* [2007]. An important issue with these new techniques is how to evaluate their performance under realistic conditions.

[5] This paper introduces a metric that can be used to assess the performance of a RFC technique. The factors that affect the performance are grouped into sea clutter, radar/system parameters, and regional meteorological statistics. As an example, the performance of RFC evaporation duct estimation is investigated for different radar frequencies and heights, three sea clutter statistics (Rayleigh, lognormal, and K-distributed), and clutter to noise ratio (CNR) values in six different littoral zones: the North Sea, Mid-Atlantic Coast, Coast of California, Mediterranean, Persian Gulf, and Coast of Brazil where ducting conditions are prevalent. Also, an evaporation duct inversion performance map of a hypothetical S band radar with radar specifications similar to the Space Range Radar (SPANDAR) is created for the larger Mediterranean/Arabian Sea region.

[6] Finally, a Bayesian version of the evaporation duct height (EDH) estimation algorithm that uses meteorological statistics as a prior density is introduced. Both the non-Bayesian [*Rogers et al.*, 2000] and the Bayesian evaporation inversion algorithms use a FFT PE [*Levy*, 2000] precomputed library of clutter profiles to estimate the EDH. These two types of RFC estimators are compared using four scenarios to show how the performance may be affected by type of the estimator.

2. Theory

[7] Let $\mathbf{m}$ be the vector containing the values of the environmental model parameters (such as the duct height, base layer thickness and slope, M deficit, inversion layer slope) that describe the true ducting environment, and $\widehat{\mathbf{m}}$ be the output of a RFC estimator that predicts the environment $\mathbf{m}$ using the observed clutter power vector $\mathbf{P^c}(\mathbf{m})$. The parameters that affect $\widehat{\mathbf{m}}$ are grouped into two categories: (1) Radar related parameters (c_r) such as the antenna gain, radar power, height and frequency that determine the signal pattern (clutter as a function of range). (2) Sea clutter parameters (c_σ) such as surface roughness, wind strength and direction, clutter statistics type, and clutter probability density function (pdf) parameters that determine the fluctuations in the received clutter signal. The interaction between each of these parameters and RFC estimation is described in detail in the following sections.

2.1. System Model

[8] Realistic replica signals received by a radar under a set of given clutter and noise statistics in a ducted environment are created using a recursive split-step FFT PE formula [*Barrios*, 1994]

$$u(z, r+\Delta r) = \exp\left[ik_{\mathrm{o}}\Delta r M(z, h_{\mathrm{d}})10^{-6}\right] \times \mathfrak{F}^{-1}\left\{\exp \cdot \left[i\Delta r\left(\sqrt{k_{\mathrm{o}}^2 - k_{\mathrm{z}}^2} - k_{\mathrm{o}}\right)\right]\mathfrak{F}\{u(z,r)\}\right\} \tag{1}$$

where $u(z, r)$ is the vertical electromagnetic field at range r, k_{o} and k_z are the wavenumber and its vertical component, Δr is the range increment in PE, $\mathfrak{F}$ and $\mathfrak{F}^{-1}$ are the Fourier and inverse Fourier transforms. The one-way propagation loss $L_{\mathbf{m}}$ in a ducted medium represented by environmental model parameter vector $\mathbf{m}$ is obtained from this electromagnetic field $u(z, r)$ [*Levy*, 2000] calculated at the effective scattering height (typically 1 m) given as 0.6 times the mean wave height [*Reilly and Dockery*, 1990]. Therefore, it is convenient to express the magnitude of the clutter signal $|E^c|$ received by the radar in terms of $L_{\mathbf{m}}$ using the classical radar equation:

$$P_k^{\mathrm{c}} = |E_k^{\mathrm{c}}|^2 = \frac{P_t G_t^2 \lambda^2 F_{\mathbf{m}}^4(r_k)\sigma_k}{(4\pi)^3 r_k^4}, \tag{2}$$

where P^{c} is the clutter power, P_t is the transmitter power, G_t is the transmit antenna gain, λ is the wavelength, σ_k is the radar cross section (RCS), r_k is the range of the range bin k, and $F_{\mathbf{m}}$ is the propagation factor (ratio of the magnitude of the electric field propagating in an environment modeled by $\mathbf{m}$ to that of free space) [*Barton*, 1988]. $L_{\mathbf{m}}$ can then be written as

$$L_{\mathbf{m}}(r_k) = \frac{L_{f_s}}{F_{\mathbf{m}}^2(r_k)} \quad \text{with} \quad L_{f_s} = \frac{(4\pi r_k)^2}{\lambda^2}, \tag{3}$$

where L_{f_s} is the free space loss. Sea surface RCS can be written as $\sigma_k = A_k\sigma^o$, where A_k is the illuminated area at bin k (proportional to r_k at small grazing angles) and σ^o is the normalized sea surface RCS or reflectivity ($\mathrm{m}^2/\mathrm{m}^2$). Then the clutter power can be written as

$$P_k^{\mathrm{c}} = \frac{P_t G_t^2 4\pi A_k \sigma^{\mathrm{o}}}{L_{\mathbf{m}}^2(r_k)\lambda^2} = C r_k L_{\mathbf{m}}^{-2}(r_k)\sigma^{\mathrm{o}}, \tag{4}$$

$$|E_k^{\mathrm{c}}| = \sqrt{P_k^{\mathrm{c}}} = c r_k^{1/2} L_{\mathbf{m}}^{-1}(r_k)\sqrt{\sigma^{\mathrm{o}}}. \tag{5}$$

where C and c account for all the constant terms [*Gerstoft et al.*, 2003]. The in-phase and quadrature components of the total received signal in a ducted environment $\mathbf{m}$ are

$$E_{\mathrm{I}}(r_k) = c r_k^{1/2} L_{\mathbf{m}}^{-1}(r_k)\sqrt{\sigma^o}\cos(\phi_k) + w_{\mathrm{I}}(r_k), \tag{6}$$

$$E_{\mathrm{Q}}(r_k) = c r_k^{1/2} L_{\mathbf{m}}^{-1}(r_k)\sqrt{\sigma^o}\sin(\phi_k) + w_{\mathrm{Q}}(r_k), \tag{7}$$

where ϕ_k is the phase of the field at the receiver, $w_{\mathrm{I}}(r_k)$ and $w_{\mathrm{Q}}(r_k)$ are the in-phase and quadrature noise components with zero mean Gaussian densities and identical variance [*Ward et al.*, 2006]. Finally, the envelope of the received signal is $|E(r_k, \mathbf{m})| = \sqrt{E_{\mathrm{I}}^2(r_k) + E_{\mathrm{Q}}^2(r_k)}$.

[9] The performance of a RFC estimator depends on how well it extracts information about the environment $\mathbf{m}$ from this radar signal $|E(r_k, \mathbf{m})|$. Therefore, it is important to determine the factors that affect each term in (6)–(7). The environmental information is included in $L_{\mathbf{m}}(r_k, \mathbf{m})$ term. Notice this term is also affected by radar/system parameters. There are two random variables: the additive noise term $w(r_k)$ and the multiplicative term $\sqrt{\sigma^{\mathrm{o}}}$ that is determined by the clutter statistics and their corresponding pdf parameters which depend mainly on the sea surface conditions, and the wind.

2.2. RFC Performance Metric

[10] A common estimator performance metric is the root mean square (RMS) error. RFC estimation performance will also be computed in terms of a weighted RMS error of the estimate $\widehat{\mathbf{m}}$ for the environment $\mathbf{m}$ given by [*Kay*, 1993]

$$e_{\widehat{\mathbf{m}}}(c_r, c_\sigma|\mathbf{m}) = E^{1/2}\left[(\widehat{\mathbf{m}}(c_r, c_\sigma) - \mathbf{m})^2\right]_{\mathbf{W}} \tag{8}$$

$$= \left(\int_{\widehat{\mathbf{m}}} [\widehat{\mathbf{m}}(c_r, c_\sigma) - \mathbf{m}]^{\mathrm{T}} \mathbf{W} [\widehat{\mathbf{m}}(c_r, c_\sigma) - \mathbf{m}] \mathrm{p}(\widehat{\mathbf{m}}|\mathbf{m}) d\widehat{\mathbf{m}}\right)^{1/2}, \tag{9}$$

where $e_{\widehat{\mathbf{m}}}$ is the RMS error, $\mathbf{W}$ is the weighting matrix that is used to nondimensionalize the parameters, and $\mathrm{p}(\widehat{\mathbf{m}}|\mathbf{m})$ is the pdf of the estimator (the distribution of the estimates $\widehat{\mathbf{m}}$ one would get from inverting for an environment $\mathbf{m}$ many times under the same set of clutter and noise statistic conditions, see section 2.4). $\mathbf{W}$ can be used also to give more weight to parameters of importance such as the duct height. A split-step FFT parabolic equation formulation is used as the forward model to relate clutter to environmental parameters. The received clutter $|E^c|$ is a nonlinear function of the environmental parameters $\mathbf{m}$ such as duct height, inversion layer thicknesses and slopes. Because of this nonlinearity, the integral cannot be analytically solved and must be numerically computed by techniques such as Monte Carlo (MC) integration [*Ó Ruanaidh and Fitzgerald*, 1996; *Yardim et al.*, 2007]. The following procedure is used to compute the error term in (9) of an RFC algorithm operating in an environment $\mathbf{m}$, noise and clutter statistics with a given clutter-to-noise ratio $\mathrm{CNR}_{r_{\mathrm{o}}}$ at the inversion start range r_{o}:

[11] 1. Compute the magnitude of the electromagnetic field $|E^c(r, \mathbf{m})|$ received by the radar as a function of range, using the split-step FFT parabolic equation for a perfect electric conductor (PEC) ocean surface at the mean wave height with a unity normalized RCS. This will give the $cr_k^{1/2} L_{\mathbf{m}}^{-1}(r_k)$ term in (5) with $\sigma^{\mathrm{o}} = 1$ and $w(r_k) = 0$.

[12] 2. Create N_{r} normalized RCS samples σ^{o} sampled from its pdf (e.g., Rayleigh, lognormal, K-distributed), and N_{r} complex Gaussian noise realizations $w(r_k)$ with N_{r} being the number of range bins used in each inversion. These two random variables are related by the given $\mathrm{CNR}_{r_{\mathrm{o}}}$ defined as:

$$\mathrm{CNR}_{r_{\mathrm{o}}} = \frac{|E_{\mathrm{o}}^{\mathrm{c}}|^2}{\langle w^2 \rangle} = \frac{C r_{\mathrm{o}} \langle \sigma^{\mathrm{o}} \rangle}{L_{\mathbf{m}}^2(r_{\mathrm{o}}) \langle w^2 \rangle}, \tag{10}$$

where $\langle \sigma^{\mathrm{o}} \rangle$ is the mean normalized RCS and $\langle w^2 \rangle$ is the noise variance. Compute the measurement vector $\mathbf{y} = [|E(r_{\mathrm{o}}, \mathbf{m})| \; |E(r_1, \mathbf{m})| \; \ldots \; |E(r_{N_{\mathrm{r}}}, \mathbf{m})|]^{\mathrm{T}}$ for $k = [0, 1, \ldots N_{\mathrm{r}}]$ using (6)–(7).

[13] 3. Invert for $\mathbf{y}$ to find the environmental estimate $\widehat{\mathbf{m}}$.

[14] 4. Repeat the previous two steps N_{MC} (number of Monte Carlo realizations) times to obtain the set of environmental estimates $\{\widehat{\mathbf{m}}_i\} = \{\widehat{\mathbf{m}}_1, \widehat{\mathbf{m}}_2, \ldots, \widehat{\mathbf{m}}_{\mathrm{MC}}\}$. Note that these samples are effectively sampled from $\mathrm{p}(\widehat{\mathbf{m}}|\mathbf{m})$ and for a sufficiently large N_{MC}, the normalized histogram of $\{\widehat{\mathbf{m}}_i\}$ converges to $\mathrm{p}(\widehat{\mathbf{m}}|\mathbf{m})$.

[15] 5. Compute the integral in (9) using the samples $\{\widehat{\mathbf{m}}_i\}$ by MC integration which can be summarized as $\int_{\widehat{\mathbf{m}}} f(\widehat{\mathbf{m}}) \mathrm{p}(\widehat{\mathbf{m}}) d\widehat{\mathbf{m}} \simeq \frac{1}{N_{\mathrm{MC}}} \sum_{i=1}^{N_{\mathrm{MC}}} f(\widehat{\mathbf{m}}_i)$ for some function $f(\widehat{\mathbf{m}})$ if the $\{\widehat{\mathbf{m}}_i\}$ are sampled from $\mathrm{p}(\widehat{\mathbf{m}})$.

[16] In addition to c_r and c_σ, the atmospheric conditions under which the radar is operating also affect the performance. These include the regional/meteorological statistics that is a function of several parameters such as the latitude, coastal/open ocean conditions, local meteorological phenomena and mesoscale atmospheric processes, the time of the day, and season/month. Each system and RFC technique has a range of values for m for which that particular RFC algorithm performs best. Hence, a system that performs well in, e.g., the North Sea may have a poor performance in the East China Sea. Therefore, in a region where the environment $\mathbf{m}$ has a meteorological statistic given by $\mathrm{p}(\mathbf{m})$, the error metric can be computed by integrating (9) over this $\mathrm{p}(\mathbf{m})$:

$$e_{\widehat{\mathbf{m}}}(\mathrm{p}(\mathbf{m}), c_r, c_\sigma) = \int_{\mathbf{m}} e_{\widehat{\mathbf{m}}}(c_r, c_\sigma|\mathbf{m}) \mathrm{p}(\mathbf{m}) d\mathbf{m}, \tag{11}$$

$$= \int_{\mathbf{m}} \left(\int_{\widehat{\mathbf{m}}} [\widehat{\mathbf{m}}(c_r, c_\sigma) - \mathbf{m}]^{\mathrm{T}} \mathbf{W} [\widehat{\mathbf{m}}(c_r, c_\sigma) - \mathbf{m}] \mathrm{p}(\widehat{\mathbf{m}}|\mathbf{m}) d\widehat{\mathbf{m}}\right)^{\frac{1}{2}} \cdot \mathrm{p}(\mathbf{m}) d\mathbf{m}. \tag{12}$$

It can be computationally expensive to compute this integral if the dimension of $\mathbf{m}$ is large since $e_{\widehat{\mathbf{m}}}(c_r, c_\sigma|\mathbf{m})$ must be computed by MC simulation for each realization of $\mathbf{m}$. However, in most cases an evaporation duct, a surface-based duct and a mixed type duct can be represented using 1, 4, and 5 parameters, respectively. Alternatively, one can only use the important parameters such as the duct height and fix the other less important values to their mean or peak values, effectively reducing the computations needed by using the marginal pdf instead of the full p($\mathbf{m}$).

2.3. Radar-Related Parameters

[17] System parameters such as the transmitted power, antenna gain, radar frequency and height affect the amount of clutter received by the radar in a ducted environment. For RFC inversion purposes the received clutter is the signal. Increasing the CNR, e.g., by increasing the transmitted power or antenna gain, will result in better RFC performance. Most RFC algorithms will not function below a certain CNR threshold. Hence, the effects of CNR on the performance and the CNR threshold calculations are carried out for CNR_{r_o} covering 5–50 dB in this paper.

[18] In addition to determining the available CNR, the system parameters such as the radar frequency and height play an important role in determining the clutter pattern in range. Taking an evaporation duct as an example, at lower frequencies and higher antennas (e.g., a S band radar such as the Space Range Radar (SPANDAR) [*Stahl and Crippen*, 1994]) the clutter caused by an evaporation duct decreases monotonically with range. However, this quickly changes to a complex pattern as the frequency is increased or the height is decreased especially for environments with large evaporation duct heights (EDH). Moreover, if the antenna is above the duct, it may not sufficiently excite the duct, resulting in a drop in CNR. The RFC performance in three typically used frequency bands, namely S, C, and X bands covering 2–12 GHz and typical naval radar heights from 5–50 m are investigated in this paper.

2.4. Sea Clutter Parameters

[19] The sea surface determines the type and strength of the sea clutter that is used in the inversion. Factors such as the wind direction and speed affect the strength of the clutter echo. It has been suggested that limited transmitted power and the noise floor can affect the RFC performance [*Rogers et al.*, 2000]. This will be addressed by analyzing the sensitivity of the RFC with varying the CNR. Moreover, the effective maximum range upon which RFC inversions can be performed is determined by the decreasing clutter power in range.

[20] In previous RFC work, sea clutter is approximated by an additive Gaussian random variable [*Gerstoft et al.*, 2003, 2004; *Vasudevan et al.*, 2007; *Yardim et al.*, 2006, 2007, 2008]. In this paper, the sensitivity of the RFC algorithm is examined using more realistic clutter statistics such as the Rayleigh, lognormal, and K-distributed sea clutter. Selection of appropriate clutter statistics for RFC applications depends on the grazing angle, surface wind speed and direction, polarization, and the size of the radar resolved area [*Long*, 2000]. In general, RFC applications are as follows:

[21] Very low grazing angle applications, less than 1° (typically less than 0.5° and 0.8° for evaporation and surface-based ducts, respectively): Grazing angles for various evaporation ducts as a function of range obtained by a ray-tracing code are given in Figure 1. The low angle results in complex scattering mechanisms such as multiple scattering and interference of scattered signals traveling in different directions, shadowing caused by the sea swells, and diffraction over the wave edges. This results in more spiky sea clutter [*Shnidman*, 1999].

[22] Low radar resolution (radar resolution cell much larger than the sea swell wavelength) applications: Even if the system is high resolution, a RFC inversion algorithm will average a number of cells to decrease the resolution. The main reason is that the field varies slowly with range and essentially is constant even within a low-resolution radar range bin. Also this reduces the CPU time, which is directly proportional to the number of range bins in split-step FFT PE. Typical range resolution values used in previous RFC applications run between 100–600 m [*Rogers et al.*, 2000; *Gerstoft et al.*, 2003, 2004; *Barrios*, 2004; *Rogers et al.*, 2005; *Yardim et al.*, 2006; *Vasudevan et al.*, 2007; *Yardim et al.*, 2007, 2008].

[23] For a low-resolution radar, a good approximation for the surface scattered field E_k^{s} at the kth radar range bin can be given simply by the superposition of the contributions from all of the N_k scatterers in that range bin [*Ward et al.*, 2006]. Assuming the radar bin is far enough, the field varies slowly across a radar bin and the magnitude of the incident field at each scatterer in the bin can be taken the same as the magnitude of the field at the center of the range bin $|E_k^i|$ giving:

$$E_k^{\mathrm{s}} = \sum_{n=1}^{N_k} a_n E^i(r_n) = |E_k^i| \sum_{n=1}^{N_k} a_n e^{j\phi_n}, \qquad (13)$$

where a_n and E_n^i are the surface reflection coefficient and the incident field, respectively, of the nth scatterer at range r_n, and ϕ_n is the relative phase that depends on factors such as the distance between the scatterer and the bin center, and the irregular sea surface structure due to the sea swell. Taking this constant $|E_k^i|$ term out of the

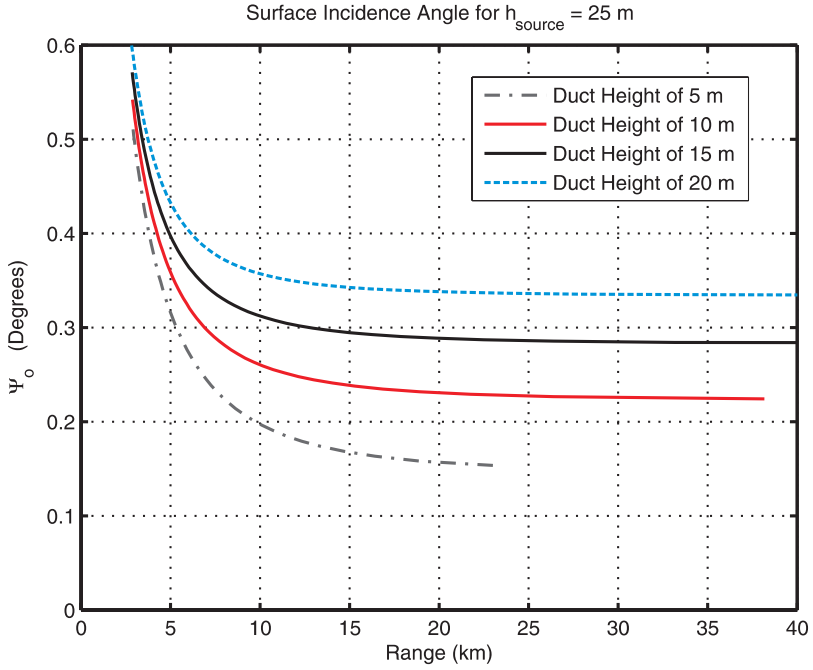

Figure 1. Grazing angle as a function of range for evaporation ducts with 5, 10, 15, and 20 m EDH.

summation, the magnitude of the leftover summation term normalized by the illuminated area of the bin A_k is be the square root of the normalized RCS $\sqrt{\sigma^o}$ given as

$$\sigma_k = \left|\frac{E_k^s}{E_k^i}\right|^2, \quad \sqrt{\sigma^o} = \frac{1}{A_k}\left|\sum_{n=1}^{N_k} a_n e^{j\phi_n}\right|. \tag{14}$$

[24] The equations (6)–(7) derived in section 2.1 use $L_{\mathbf{m}}$ obtained from the split-step FFT PE calculations. This means we use the total field at the scattering height instead of the incident field E^i as suggested by (14). However, this usually is not problematic since RFC algorithms are only interested in the relative variation of the clutter with range. Assuming the ratio between the incident and total fields does not vary too much, this is a good approximation as shown by *Dockery* [1990] and *Konstanzer et al.* [2000]. In most RFC applications the incidence angle is very small and there are few propagating modes. Nevertheless, the cases that involve large duct formations and high radar frequencies will result in the propagation of many significant modes. For these cases, the relation between incident and total field can be complex. In such cases, one must use the incident field itself that can be obtained by algorithms such as the one given by *Konstanzer et al.* [2000]. Such an approach would also enable us to use a more complicated expression for the backscattered energy. In RFC theory, the backscattered energy is assumed independent of the incident grazing angle and the ranges upon which inversion is carried out are restricted to regions where the incident angle is almost constant to minimize any potential error. All the simulations in this paper are carried out using standard PE calculations and the total field.

[25] As the radar resolution decreases, A_k increases and hence the number of random scatterers N_k inside the bin increases. Therefore, unless the grazing angle is very low, the summation in (14) becomes Gaussian as dictated by the Central Limit Theorem and $\sqrt{\sigma^o}$ becomes a Rayleigh reducing the spiky behavior [*Skolnik*, 2001].

[26] To take these two phenomena (very low grazing angle and low radar resolution) into account, three sea clutter statistics are used and compared in this paper. To prevent any confusion with the standard deviation and variance notations the random variable x is used for clutter amplitude ($\sqrt{\sigma^o}$) and X for normalized RCS (σ^o):

[27] 1. Rayleigh: Rayleigh statistics are suitable in applications with high grazing angle (>10°) and low radar resolution [*Ward et al.*, 2006]. The pdf complex Gaussian, which corresponds to Rayleigh amplitude statistics with

$$\mathrm{p}(x) = \frac{2x}{\langle X\rangle}\exp\left(\frac{-x^2}{\langle X\rangle}\right), \tag{15}$$

Table 1. K Distribution Shape Parameter for Different Scenarios

Scenario	A	B	C	D
Range (km)	10	20	15	20
Azimuth Beam Width (deg)	0.5	1.0	0.4	2.0
Range Resolution (m)	100	150	200	500
Grazing Angle (deg)	0.5	0.2	0.2	0.5
Polarization Parameter	2.09	2.09	1.39	1.39
Swell Angle (deg)	0	0	0	90
Shape Parameter (ν)	0.69	1.15	3.20	161

where x is the clutter amplitude and $\langle x^2 \rangle = \langle X \rangle$. The spikiness of the clutter is given by its normalized RCS mean-to-median ratio $\langle X \rangle / X_m$. The Rayleigh pdf has a fixed $\langle X \rangle / X_m = 1.6$ dB.

[28] 2. Lognormal: The lognormal pdf is used to describe spiky sea clutter. Although this pdf does not explain the underlying physics of the sea clutter, its pdf with a long tail fits well to spiky clutter measurements that are encountered in low grazing angle applications. The pdf of the lognormal distributed RCS is given by

$$\mathrm{p}(X) = \frac{1}{X\sigma\sqrt{2\pi}} \exp\left(-\frac{(\ln(X)-\mu)^2}{2\sigma^2}\right), \qquad (16)$$

where μ and σ are the mean and the standard deviation of the Gaussian function in the logarithmic domain. The mean-to-median ratio in dB is $0.115\sigma_{\mathrm{dB}}^2$ with a high value corresponding to a spiky clutter [*Long*, 2000].

[29] 3. Compound K distribution: The K distribution was introduced as an effective means to represent the sea clutter amplitude [*Jakeman and Pusey*, 1976]. Later, its compound nature and the underlying physical mechanisms that enable the splitting of this complex pdf into two distinct components were demonstrated by *Ward* [1981]. The K distribution is used extensively in applications with high radar resolution and grazing angles as low as 0.1° [*Ward et al.*, 2006].

[30] The K distribution is a compound pdf where the gamma distributed local mean normalized RCS p(X) is modulated by the fast changing Rayleigh speckle p($x|X$). The gamma component represents the slowly varying swell structure. The clutter amplitude statistics p(x) can be obtained as [*Ward et al.*, 2006]

$$\mathrm{p}(X) = \frac{b^\nu}{\Gamma(\nu)} X^{\nu-1} \exp(-bX), \quad \mathrm{p}(x|X) = \frac{2x}{X} \exp\left(\frac{-x^2}{X}\right), \qquad (17)$$

$$\mathrm{p}(x) = \int_0^\infty \mathrm{p}(x|X)\mathrm{p}(X)dX = \frac{4b^{1/2}}{\Gamma(\nu)} (bx)^\nu K_{\nu-1}\left(2x\sqrt{b}\right), \qquad (18)$$

where $\Gamma(\nu)$ is the Gamma function, b and ν are the scale and shape factors with the mean normalized RCS $\langle X \rangle = \nu/b$, and $K_{\nu-1}$ is the modified Bessel function of the third kind of order $\nu-1$. The shape parameter ranges from $0.1 \leq \nu \leq \infty$ and determines the spikiness of the pdf; $\nu < 1$ represents spiky clutter and $\nu = \infty$ reduces the K distribution to a Rayleigh.

[31] Depending on the radar and environmental parameters, all three distributions can be encountered for the RFC application. Because of the low-resolution nature of the RFC techniques, very spiky clutter is less likely to be encountered in RFC applications. However, a pure Rayleigh approach may be too optimistic in many cases. As shown by *Chan* [1990], even at low resolutions, the low grazing angle situations result in mildly spiky K distributions. Therefore, RFC performance under all three clutter statistics is investigated for the evaporation duct RFC estimator. Typical values of ν are given in Table 1 using the empirical model developed for X band [*Ward et al.*, 2006]

$$\log(\nu) = \frac{2}{3}\log(\Psi_{\mathrm{o}}) + \frac{5}{8}\log(A_k) - k_{\mathrm{pol}} - \frac{1}{3}\cos(2\theta_{\mathrm{sw}}), \qquad (19)$$

where Ψ_{o}, A_k, k_{pol}, and θ_{sw} are the grazing angle in degrees, radar resolved area, polarization parameter ($k_{\mathrm{pol}} = 1.39$ for VV and $k_{\mathrm{pol}} = 2.09$ for HH), and angle with respect to the swell direction. The four scenarios (Table 1) show the spectrum of possible shape parameters from the spiky clutter of scenario A to almost Rayleigh clutter of scenario D. For most RFC applications, the clutter is expected to be mildly to weakly spiky with $\nu = 1-5$.

[32] To compare all three clutter densities under the same set of conditions, the same mean normalized RCS ($\langle \sigma^{\mathrm{o}} \rangle$ or $\langle X \rangle$), $\mathrm{CNR}_{r_{\mathrm{o}}}$, and mean-to-median ratio $\langle X \rangle / X_m$ are used during the simulations. For a given $\mathrm{CNR}_{r_{\mathrm{o}}}$ and $\langle X \rangle$ the variance of the additive noise term is calculated from (10). After the shape parameter ν is selected for a desired level of spikiness ($\langle X \rangle / X_m$), the scale factor b is obtained using $\langle X \rangle = \nu/b$. Unless otherwise stated, a value of $\nu = 1$ is used in the K-distributed clutter simulations.

2.5. Environment: Regional Meteorological Statistics

[33] Factors such as the complex local and global atmospheric processes, proximity to land, and latitude difference influence duct statistics. Each RFC inversion technique will have different environmental parameter intervals within which they perform best. To take these variations into account a worldwide surface meteorological observations database sponsored by the SPAWAR Systems Center, San Diego (SSC-SD) was created. The environmental library of the Advanced Refractive Effects Prediction System (AREPS) [*Patterson*, 2005] created

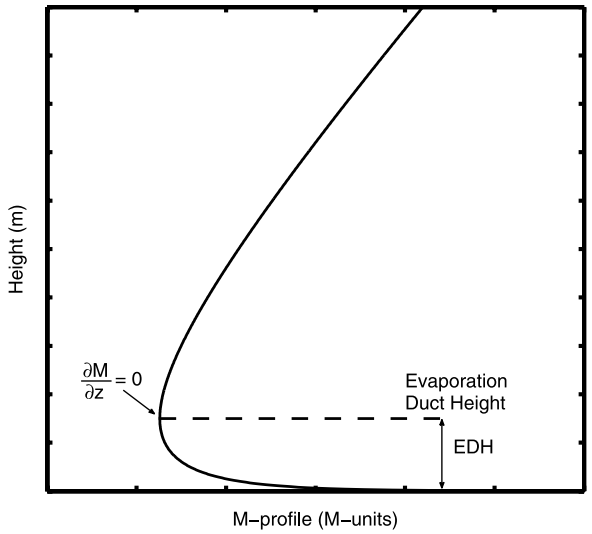

Figure 2. Vertical M profile for an evaporation duct. Trapping occurs between the sea surface and the evaporation duct height (EDH).

over 293 10° × 10° sections of the world between 80°N and 70°S latitudes called Marsden Squares (MS) is used here.

3. Performance Analysis for Evaporation Duct RFC Estimator

[34] The factors that affect the RFC performance are explained using an evaporation duct RFC estimator that inverts for the evaporation duct height (EDH) as an example. An evaporation duct RFC estimation is selected since the performance can be examined world wide thanks to the availability of detailed global meteorological statistics for EDH in AREPS environmental library [*Patterson*, 2005]. For an evaporation duct the dimension of **m** is 1, enabling us to examine the method in detail. In order to address separately the effects of the factors mentioned in section 2, three performance analyses are carried out analyzing the effects of clutter statistics/CNR, the radar height/frequency, and the regional meteorological statistics. Finally, these are merged to compute the evaporation duct estimator performance map of an S band radar for the larger Mediterranean/Arabian Sea region.

3.1. Evaporation Duct Inversion Algorithm

[35] Evaporation duct refractivity profiles are constructed using the log linear evaporation duct formula given by *Paulus* [1990]. Following *Rogers et al.* [2000], only the evaporative duct height (EDH) is used in the formulation, assuming the air and sea surface temperatures are almost identical with a neutrally buoyant boundary layer. As shown in Figure 2, EDH defines the upper boundary of the trapping layer where $\partial M/\partial z = 0$. Hence, the M profile is given by

$$M(z, h_d) = M_0 + c_o\left(z - h_d \ln\frac{z + z_o}{z_o}\right), \qquad (20)$$

where h_d represents the EDH, M_0 is the refractivity at the sea surface, the constant c_o and the roughness factor z_o are taken as 0.13 M-units/m and 1.5×10^{-4} m, respectively.

[36] Evaporation duct inversion consists of minimizing the RMS error between the measured clutter with those in a precomputed clutter library in a given range interval. The library typically consists of clutter patterns that would be encountered for EDH ranging from 0–40 m. Sea clutter in a ducted environment is obtained using the split-step FFT PE and calculated as given in (4). The clutter library for a given RFC algorithm for a range $[r_o, r_f]$ is constructed from the normalized clutter $P_n(r, h_d) = P^c(r, h_d) - P^c(r_o, h_d)$ in dB. Since the signal level is higher at shorter ranges (higher CNR), the selection of a smaller r_o improves RFC performance. However, it is desirable to perform the inversion in an interval where the grazing angle is nearly constant which requires a larger r_o. Therefore, r_o is selected as a compromise between these two opposing requirements. The relationship between grazing angle and clutter for very low angle conditions in ducted environments is still an active discussion in the literature [*Barrick*, 1998; *Tatarski and Charnotskii*, 1998; *Rogers et al.*, 2000]. The minimum range where the grazing angle becomes constant for a launching elevation angle in an evaporation, surface-based, or mixed type duct can be found using ray tracing [*Paulus*, 1990; *Rogers et al.*, 2000]. Since this range depends on the unknown environmental parameters, a value slightly more conservative than the one obtained for the mean M profile expected in the region can be used. Without loss of generality, r_o is taken here as 10 km. The final range r_f of the inversion interval is dictated by CNR with values between 20–25 km used in this work. Here a constant r_f is used but an adaptive method where r_f is determined based on the available CNR can also be used. The noise floor is modeled similar to the one given by *Rogers et al.* [2005]. The clutter curves in the libraries are first normalized for a given CNR_{r_o} and then truncated for values less than 0 dB. The truncated libraries for a clutter-to-noise ratio at 10 km $CNR_{10} = 40$ dB are given in Figure 3. The received noisy signal is then compared to these truncated libraries. Note that the selection of r_f and how the noise floor is handled may affect significantly the performance of any RFC algorithm.

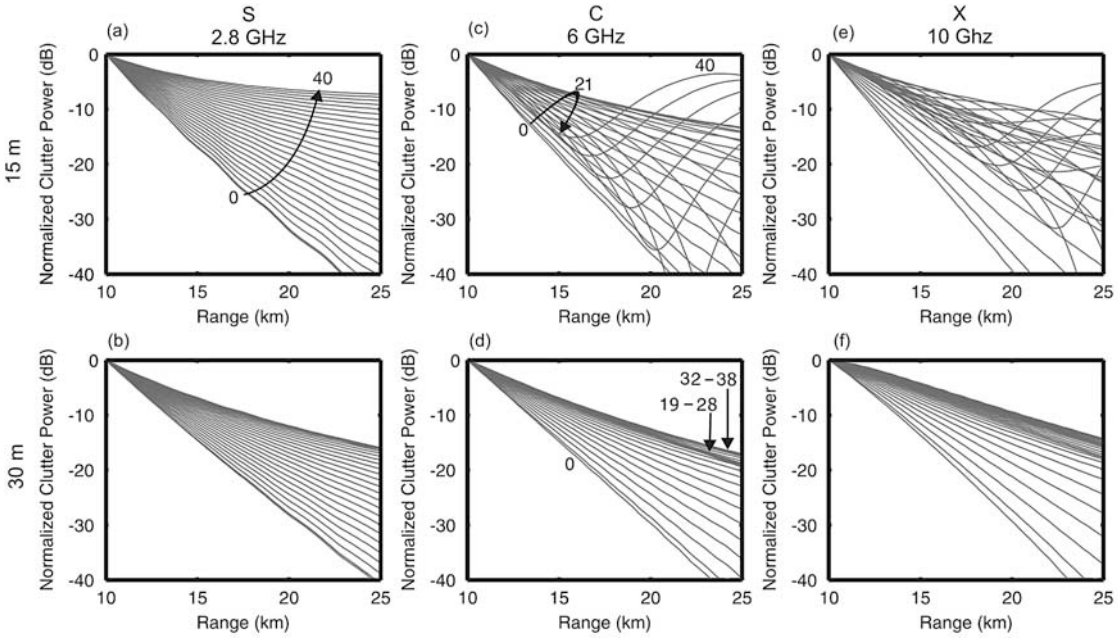

Figure 3. Normalized clutter libraries of evaporation ducts with EDH ranging from 0 to 40 m for three frequencies and two antenna heights: (a) 2.8 GHz, 15 m, (b) 2.8 GHz, 30 m, (c) 6 GHz, 15 m, (d) 6 GHz, 30 m, (e) 10 GHz, 15 m, and (f) 10 GHz, 30 m. Arrows show the evolution of the clutter pattern as EDH increases.

[37] The EDH is estimated by minimizing the error function $\phi(h_d)$ between the library-stored normalized clutter $P_n(r, h_d)$ with the normalized radar-measured clutter $P_m(r)$:

$$\phi(h_d) = \sum_{r=r_o}^{r_f} [P_n(r, h_d) - P_m(r)]^2 \qquad (21)$$

3.2. Evaporation Duct Estimator Performance

[38] The structure and variation of the clutter library of an evaporation duct RFC algorithm determine how well it will perform in a given environment. Six libraries between 10–25 km range are shown in Figure 3 with different radar frequencies and antenna heights.

[39] Clutter libraries of S band (2–4 GHz) radars typically consist of monotonically increasing radar return profiles as EDH increases as given in Figures 3a and 3b. As the radar height increases the vertical spread of the library decreases, resulting in a loss of sensitivity to different EDHs. Analysis in the work of *Rogers et al.* [2000] indicates that RFC is difficult for EDH > 30 m in S band. However, this value is frequency and antenna height dependent (can be as low as 5 m) and clutter libraries get considerably more complex as the frequency increases.

[40] Libraries corresponding to a 6 GHz radar are provided in Figures 3c and 3d. As EDH is increased, the clutter patterns is dominated by constructive/destructive interference. For a radar height of 15 m, the clutter monotonically increases from 0–21 m EDH after which it again starts to decrease and becomes a complex pattern. For a radar height of 30 m, the clutter monotonically increases from 0–40 m but for EDH between 19–28 m and 32–38 m the clutter pattern is almost identical, drastically reducing the inversion quality. These effects get more pronounced for X band simulations.

[41] Radar frequency and height affect heavily the clutter library of the evaporation duct and thus result in large variations in RFC performance. The inversion statistics for EDH values for the libraries in Figures 3b and 3c are shown in Figure 4. Figure 4 provides histograms of the inversion results for 1000 inversions for duct height values of 1, 5, 10, 15, 20, 25, 30, 35, and 40 m. The S band radar (Figure 4a) performs well up to an EDH of around 30 m with only n_{avg} = 10. The performance degrades at higher values due to the similar clutter patterns of the environments with large EDH values, reducing the sensitivity of the inversion. The C

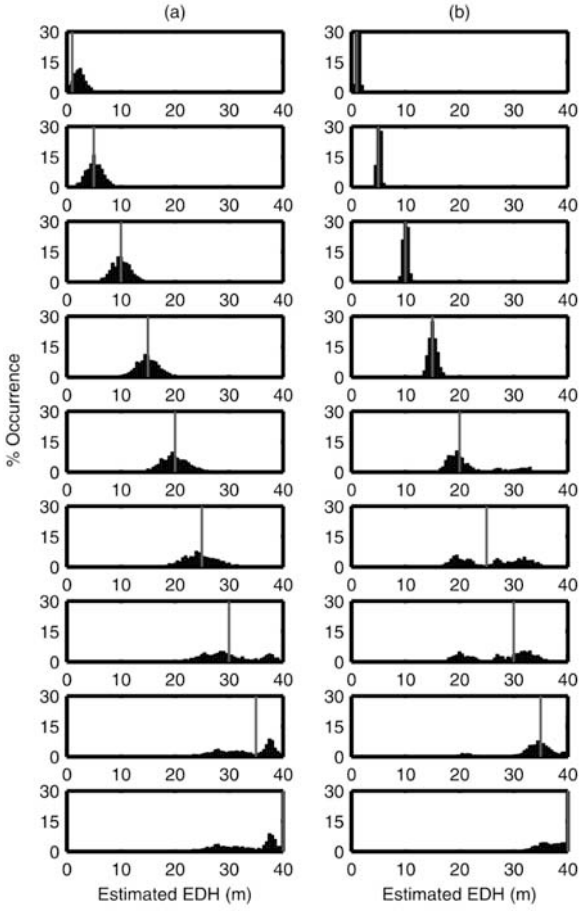

Figure 4. Evaporation duct inversion algorithm performance. Histograms representing $p(\hat{\mathbf{m}}|\mathbf{m})$ under K-distributed clutter with 40 dB CNR_{r_o}. (a) $f = 2.8$ GHz, 30 m antenna height, $n_{avg} = 10$ and (b) $f = 6$ GHz, 15 m antenna height, $n_{avg} = 100$. Vertical lines show the true EDH, **m**.

band radar (Figure 4b) performs better than the S band radar up to 20 m, with a smaller variance due to both the faster variation between the clutter patterns as EDH increases for low EDHs (compare Figures 3b and 3d) and the selection of $n_{avg} = 100$. However, due to its complex library patterns, the performance degrades considerably between 20–30 m and then increases again for larger duct heights.

[42] The nonlinear EDH performance characteristic in Figure 5 shows how radar systems with frequencies from 2–12 GHz and antenna heights of 5–50 m performs for a given EDH. For small EDH values, most frequency-height combinations work well. As EDH increases certain regions perform better than others and these regions shift with EDH except for the low frequency/low radar height combination. Also note that regions with poor performance start to appear as early as a duct height of only 5 m. Since the performance of each frequency-height value depends on the actual EDH of the environment it is operating in, regional statistics also must be incorporated to give a true performance metric for a RFC technique.

[43] Sea surface and other radar parameters determine the clutter statistics and the clutter echo strength (hence the CNR). Figure 6 shows the RMS error in the inversion of an evaporation duct with an EDH of 20 m for a CNR_{r_o} ranging from 5–50 dB at the inversion start range (r_o = 10 km) and for clutter with different mean-to-median ratios. The ν values of the K distribution are selected to give identical $\langle X \rangle / X_m$ and mean normalized RCS $\langle X \rangle$ as the lognormal simulations. The frequency and the antenna height correspond to those of SPANDAR (2.8 GHz and 31 m). The signal is constructed by averaging ten consecutive clutter returns ($n_{avg} = 10$), and the RMS error is based on 5000 simulations.

[44] Below 10 dB CNR_{r_o}, the signal is entirely noise-dominated and the performance quickly degrades. When the noise level is too high, the algorithm fails to correctly normalize the measured clutter, resulting in large errors in the RFC estimates. Similarly, above about 20–25 dB CNR_{r_o}, the effects of noise are negligible and an infinite CNR_{r_o} assumption can be used since the received signal is clutter dominated and the performance rapidly converges to the infinite CNR_{r_o} case.

[45] The spiky clutter requires a higher CNR_{r_o} to attain the same RMS error and the infinite CNR_{r_o} error values are larger compared to the less spiky clutter. Note that a transitional region exists between the noise-dominated and clutter-dominated CNR_{r_o} spectrum. This transitional region starts at a low CNR_{r_o} for clutter with a low mean-to-median ratio and is sharper. For highly spiky clutter with $\langle X \rangle / X_m = 8$ dB, the required CNR_{r_o} to reach the clutter-dominated region is as high as 35 dB.

[46] As shown in Figure 6, SPANDAR with a 40 dB CNR_{r_o} is affected minimally by the noise. However, few naval radar systems have the antenna gain or the power of SPANDAR. A typical naval radar would attain a CNR_{r_o} around 20–25 dB at 10 km [*Rogers et al.*, 2000]. For less spiky clutter at this CNR_{r_o} range, the performance is close to that of the asymptotic infinite CNR_{r_o} case. However, for spiky clutter, this CNR_{r_o} may not be enough. In those cases, a large number of averages is needed, especially taking long correlation times of the gamma distributed component of the K distribution into account. Therefore it is important that a CNR_{r_o} performance analysis be carried out to find the minimum CNR_{r_o} needed for a given RFC algorithm.

[47] The occurrence rates and strength of evaporation ducts vary depending on the region, season, time of the day, and regional atmospheric processes. Factors such as

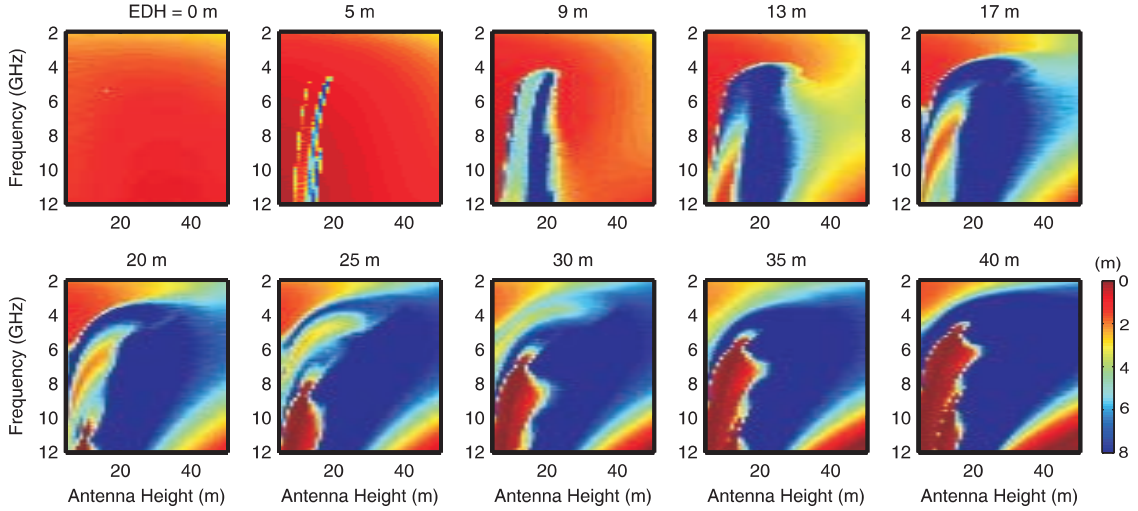

Figure 5. Performance plots: RMS evaporation duct height error as a function of radar frequency and antenna height in environments with duct heights ranging from 0 to 40 m for K-distributed clutter with CNR_{r_o} = 40 dB and n_{avg} = 10.

day versus night, summer versus winter, and low latitude versus high latitude that increase evaporation from the sea surface generally result in stronger ducts.

[48] The six cases (Env-1 to Env-6) investigated here are given in Figure 7. Selected regions, seasons, and time of day information is provided in Table 2 along with the mean EDH and surface wind speed values. They represent a wide spectrum of environments with different mean and statistics for the EDH, and hence different RFC performance. The cases are ranked according to their mean EDHs so they start with the North Sea with a mean EDH of only 4.8 m due to its relatively high latitude. The first two (Env-1 and Env-2) pdfs resemble a truncated Gaussian whereas Env-3 and Env-6 have Gaussian pdfs with different means, Env-4 has a high variance and a high pdf value at low EDH disrupting the Gaussian nature, and Env-5 has a non-Gaussian pdf with a long tail toward the high EDH values. These statistics are then used in performance calculations.

[49] Surface wind speed statistics also are provided in Figure 7b. This paper does not directly address the effects of wind. However, some important aspects are indirectly addressed. One example is the low wind speed case (0–2 m/s [*Rogers et al.*, 2000]), which results in flat sea surface, significantly reducing the backscattering and hence, degrading RFC performance. This would correspond to the low CNR case in Figure 6. Env-5 is affected most from this due to the high occurrence percentage of low surface wind speed conditions in the Persian Gulf (Figure 7b).

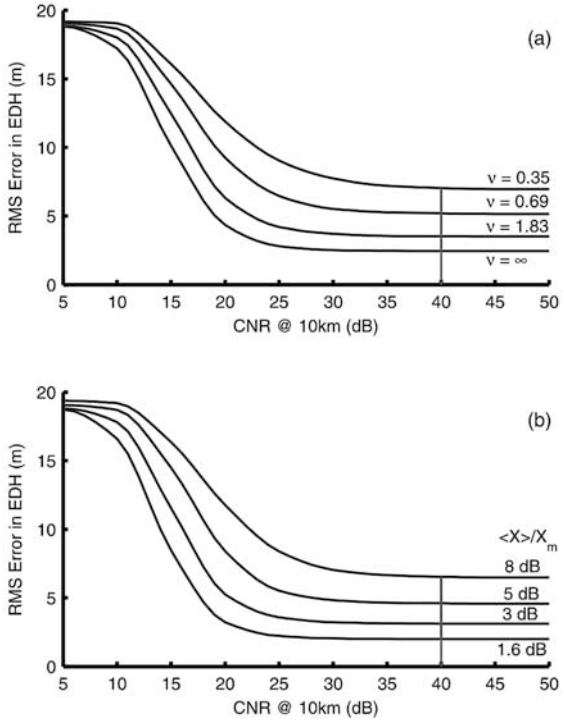

Figure 6. Performance plots: RMS evaporation duct height error for a 20 m high evaporation duct as a function of CNR_{r_o} for (a) K-distributed and (b) lognormal clutter, with mean-to-median ratios of 1.6 (where K distribution reduces to a Rayleigh), 3, 5, and 8 dB. Vertical lines represent a 40 dB CNR_{r_o} that can be attained by the Space Range Radar (SPANDAR).

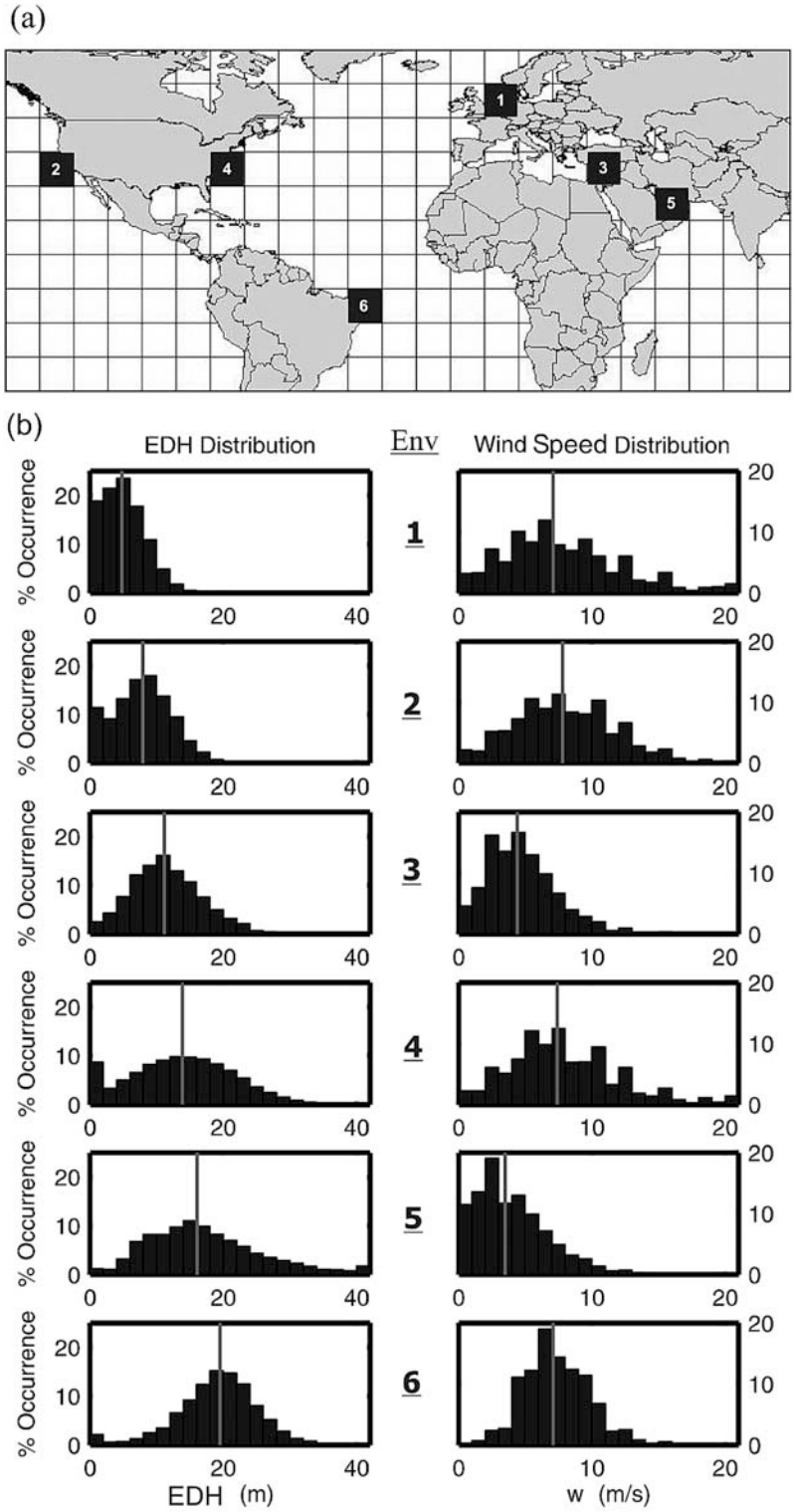

Figure 7. Regional statistics for (a) six different regions/seasons/time of the day (see Table 2) in terms of (b) evaporation duct height and surface wind speed; vertical lines show the mean values.

Table 2. Regional Environmental Statistics

Environment	Marsden Square	Region	Season	Time	Mean EDH (m)	Wind (m/s)
Env-1	MS-216	North Sea	Spring	Day	4.8	7.1
Env-2	MS-121	Coast of California	Summer	Night	7.9	7.8
Env-3	MS-141	East Mediterranean	Spring	Day	11.2	4.8
Env-4	MS-116	Mid-Atlantic Coast	Spring	Day	13.9	7.4
Env-5	MS-103	Persian Gulf	Fall	Day	16.1	3.5
Env-6	MS-303	Coast of Brazil	Fall	Day	19.5	7.1

[50] Another case arises when the sea surface wind speed is high. This results in rough sea conditions, significantly altering the clutter statistics and properties such as the spikiness, which has a major effect on RFC performance. This also is addressed by simulating clutter statistics with high mean-to-median ratios. Env-1, Env-2, and Env-4 will be affected most from spiky clutter (Figure 7b).

[51] Finally it should be noted that, the wind conditions and the clutter statistics are assumed to be uniform in range. The sensitivity analysis for range varying clutter statistics is not included in this work. These range variations typically are larger in coastal areas than the open ocean conditions where they tend to be more uniform. *Rogers et al.* [2000] averages the received clutter around multiple azimuths to minimize the effects of range variation on the RFC inversion.

[52] The performance computed using (12) is plotted in Figure 8 for Env-1, Env-3, and Env-6 from Table 2. Comparing Figure 8a with Figure 8c, it can be concluded that RFC performance is a strong function of the regional statistics. Most frequency-height combinations work well in Env-1 whereas they must be selected carefully for Env-6. For example, the SPANDAR radar (“pluses” in Figure 8 at 2.8 GHz, 31 m) is a good choice for Env-1 and Env-3 but performance is only mediocre in Env-6.

[53] RMS error of all 6 environments (Table 2) for 5 frequency heights are given in Table 3. The low frequency–low height system gives the best RMS errors for all 6 environments with a small variation in performance from region to region. On the contrary, the RMS error of the 8 GHz system varies from 2.3–11.2 m. Also note how SPANDAR performs better in the first three environments, whereas the 10-GHz/10-m system works better in the last three.

[54] The final example shows a RFC performance map of the larger Mediterranean/Arabian Sea region for the SPANDAR radar (Figure 9). It is obtained again using (12) where day/night averaged annual statistics for each Marsden Square (MS) are used to compute the performance and values between are interpolated. Noticeable features include the large RMS error in the Red Sea, larger errors in Indian Ocean with respect to the Eastern Atlantic Ocean with similar latitudes, and decreasing performance from West to East Mediterranean. Note the correlation between the performance pattern and the

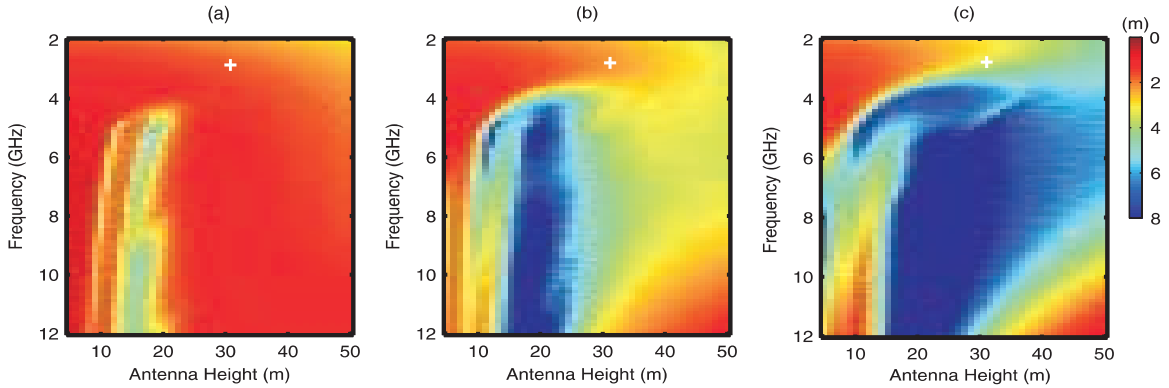

Figure 8. Performance plots: RMS error integrated over the regional statistics: (a) Env-1, (b) Env-3, and (c) Env-6. The “pluses” indicate the frequency and the antenna height of the Space Range Radar (SPANDAR).

Table 3. RMS Error of Five Frequency-Height Values for the Environments Given in Figure 7 and Table 2

RMS Error (m)	2.8 GHz 31 m	3 GHz 10 m	6 GHz 15 m	8 GHz 20 m	10 GHz 10 m
Env-1	1.8	1.3	2.3	2.3	1.9
Env-2	1.9	1.3	3.6	5.4	2.6
Env-3	2.2	1.3	4.5	8.6	2.9
Env-4	2.7	1.5	4.1	8.8	2.4
Env-5	3.1	1.5	4.4	10.0	2.4
Env-6	3.5	1.6	4.3	11.2	2.2

mean EDH (from west to east: 9.8, 10.6, 11.3, 12.5, and 12.4 m) of the regional statistics in the Mediterranean.

4. A Bayesian Approach to RFC Inversion

[55] The performance can be improved using a Bayesian estimator that takes advantage of the regional statistics given in the previous section. It can use the same Bayesian RFC approach applied by *Yardim et al.* [2006, 2008] where the posterior probability density (PPD) of EDH is obtained by multiplying the likelihood function, which carries the information obtained from clutter, by the prior density, which is the pdf of the EDH statistics encountered in that region (Figure 7). Afterward, a maximum a posteriori (MAP) estimator which computes the peak of the PPD can be employed.

[56] To demonstrate the advantages and drawbacks of the Bayesian approach, a simplified formulation that assumes zero-mean Gaussian error between the measured and modeled clutter is given. Since the clutter is represented in dB, this assumption corresponds to a lognormal clutter with infinite CNR. The MAP estimate $\widehat{h}_\mathrm{d}$ can be found by

$$\mathcal{L}(h_\mathrm{d}) = \left(2\pi\sigma^2\right)^{-N_\mathrm{R}/2} \exp\left[-\frac{\phi(h_\mathrm{d})}{2\sigma^2}\right], \tag{22}$$

$$\mathrm{p}(h_\mathrm{d}|P_m) = \frac{\mathrm{p}(h_\mathrm{d})\mathcal{L}(h_\mathrm{d})}{\int_{h'_\mathrm{d}} \mathrm{p}(h_\mathrm{d})\mathcal{L}(h_\mathrm{d})\mathrm{d}h'_\mathrm{d}}, \tag{23}$$

$$\widehat{h}_\mathrm{d} = \arg\max_{h_\mathrm{d}} \mathrm{p}(h_\mathrm{d}|P_m), \tag{24}$$

where $\mathcal{L}(h_\mathrm{d})$ is the likelihood function created from the error function $\phi(h_\mathrm{d})$, N_R is the number of range bins in the inversion range interval, $\mathrm{p}(h_\mathrm{d})$ is the regional prior, the probability of EDH given the measured clutter $\mathrm{p}(h_\mathrm{d}|P_m)$ is the PPD, and σ^2 is the error variance given in (16). A high σ^2 means a highly spiky lognormal clutter with the mean-to-median ratio given in section 2.4. [*Anderson*, 1995] shows that a variation of up to 10 dB can be observed in ranges in excess of 10 km. Assuming a modest averaging, the values used in the simulations here are selected as given in Table 4.

[57] Four cases are simulated for comparison, see Table 4; the priors $\mathrm{p}(h_\mathrm{d})$ are selected from Figure 7. The inversion results are given in Figure 10. Because of the monotonic variation in the clutter patterns (Figure 3b), $\phi(h_\mathrm{d})$ has a single minimum (Figure 10a). The PPD is

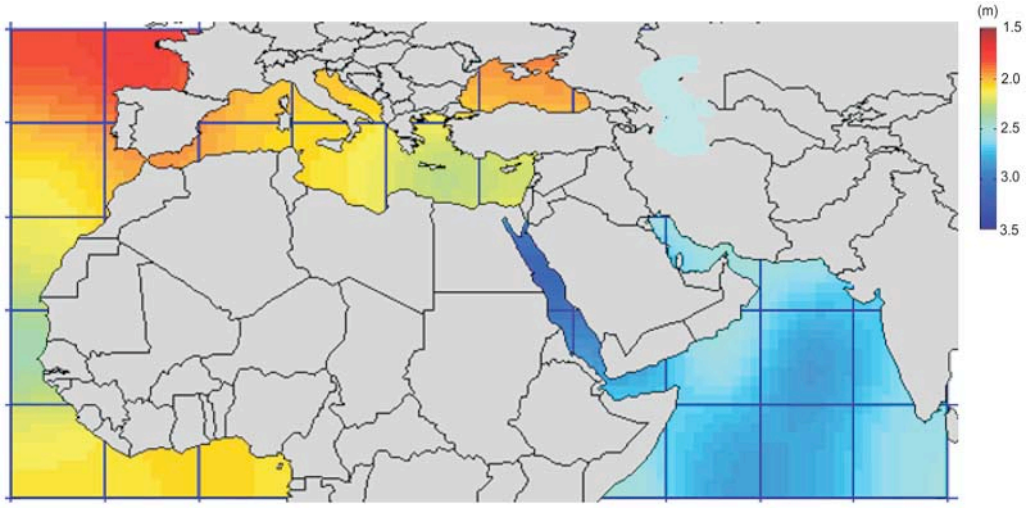

Figure 9. Performance map of the East Atlantic Coast, Mediterranean, Persian Gulf, Red Sea, Black Sea, and the Arabian Sea. RMS evaporation duct height error for SPANDAR operating with CNR_{r_o} = 40 dB and a K-distributed sea clutter and n_{avg} = 10.

Table 4. Simulation Parameters Used in Figure 10

	(a)	(b)	(c)	(d)
Prior	Env-1	Env-3	Env-4	Env-5
Radar Frequency (GHz)	2.8	6	6	10
EDH (m)	10	15	30	35
CNR (dB)	∞	∞	∞	∞
Radar Height (m)	30	15	15	15
Lognormal Clutter SD (dB)	3	3	5	5

obtained by multiplying the likelihood with the prior of Env-1 and a MAP estimator finds the EDH corresponding to the maximum of the PPD. Both the Bayesian and the non-Bayesian approaches work well for this case.

[58] An advantage of a Bayesian approach is demonstrated in Figure 10b. A complex clutter library results in multiple possible solutions with a $\mathcal{L}(h_d)$ having three local maxima. The two incorrect values are removed in the PPD due to the prior. The final value obtained from the MAP estimator is accurate. However, the same mechanism picks a wrong value for the third case shown in Figure 10c. The prior reduces the peak with the true EDH and the subsequent MAP estimation results in an incorrect estimate, whereas the non-Bayesian algorithm estimates the true value of the EDH. However, based on the priors, case (b) is much more likely than case (c) in that environment, hence, the Bayesian algorithm could mask rare events with low probability even though the overall performance is improved.

[59] The final example given in Figure 10d shows how both techniques may fail if the system parameters are not carefully selected by a performance analysis similar to the one in Figure 8. Both $\phi(h_d)$ and the PPD show possible solutions around 5, 21, and 35 m EDH even

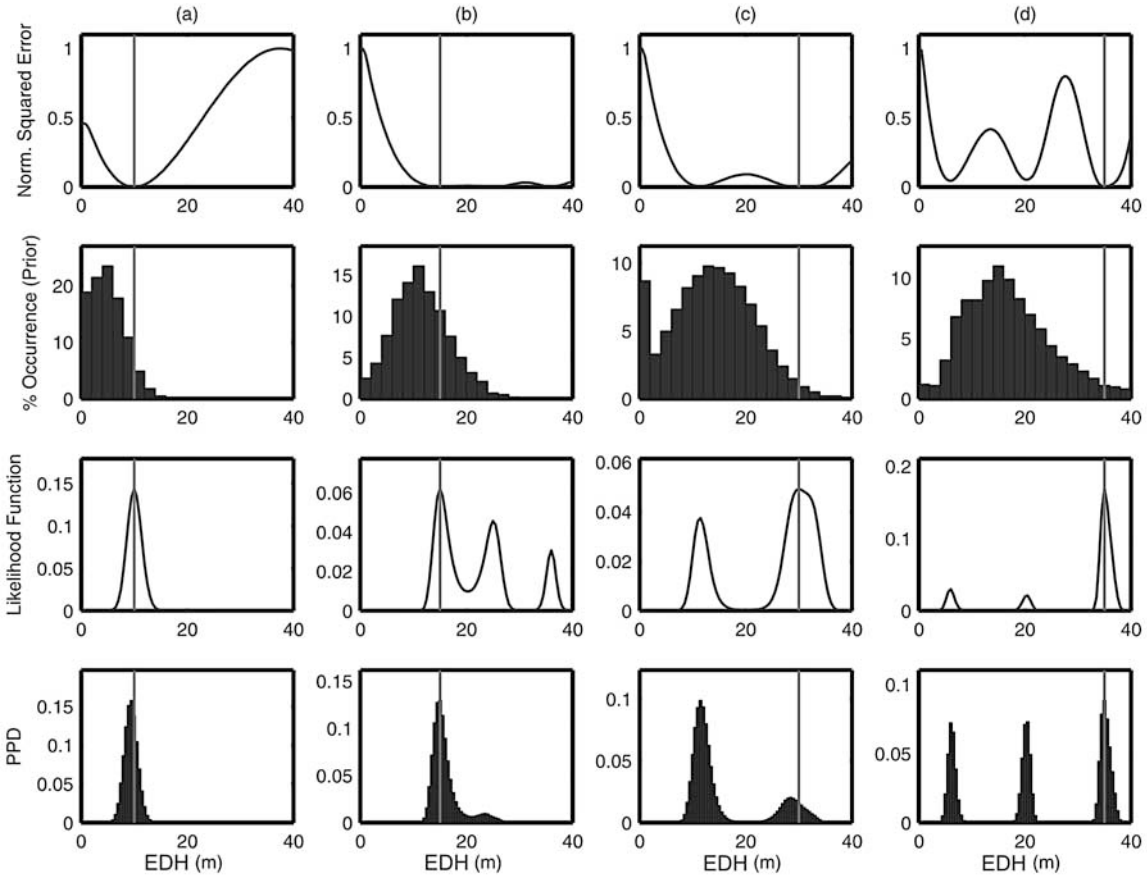

Figure 10. Evaporation duct inversion results for cases given in Table 4. Error function $\phi(h_d)$ used in inversion along with the prior $p(h_d)$ (regional statistics), likelihood $\mathcal{L}(h_d)$ obtained from the error function, and the posterior probability density (PPD) $p(h_d|P_m)$. Vertical lines show the true EDH.

with an infinite CNR. Thus, the selected system parameters are not appropriate for Env-5, the Persian Gulf. Note, however, that it might work well in the North Sea. Because of this nonlinearity, the integral cannot be analytically solved and must be numerically computed by techniques such as Monte Carlo (MC) integration. It is highly unlikely that ducts with high EDH values will be encountered in Env-1.

5. Conclusion

[60] The purpose of refractivity from clutter (RFC) is to extract the refractivity directly from the radar clutter return. To access the RFC technique a performance metric was introduced to compute the RMS RFC estimator error. Using this performance metric, the effects of the strength of the clutter echo (analyzed as a function of CNR), selection of suitable clutter statistics for RFC applications, the effects of the clutter library due to system parameters such as the radar frequency and antenna height, and meteorological statistics were discussed.

[61] Performance calculations on an evaporation duct RFC estimator were provided. These included RFC performance for different regions and creation of performance maps. The example showed that the performance is a strong function of radar frequency and height for the evaporation duct estimator. The RFC performance degraded as the clutter became more spiky, both for the lognormal and K-distributed clutter return. Estimator performance for six regions showed how radar parameters/RFC algorithm selection affected the performance.

[62] Finally, a Bayesian evaporation duct RFC estimator was introduced and a performance comparison between Bayesian and non-Bayesian RFC estimators was made. The results showed how performance can be improved with the inclusion of meteorological statistics within the RFC estimation algorithm in most cases while the extreme ducting events may be missed by the Bayesian algorithm.

[63] **Acknowledgments.** The authors would like to thank to Ted Rogers and Amalia Barrios from SPAWAR, San Diego, California, D. Dockery, Applied Physics Laboratory, Johns Hopkins University, Baltimore, Maryland, and Hank Owen for their helpful discussions. This work was supported by the Office of Naval Research under grant N00014-05-1-0369.

References

Anderson, K. D. (1995), Radar detection of low-altitude targets in a maritime environment, *IEEE Trans. Antennas Propag.*, *43*(6), 609–613.

Barrick, D. E. (1998), Grazing angle behavior of scatter and propagation above any rough surface, *IEEE Trans. Antennas Propag.*, *46*(1), 73–83.

Barrios, A. (2004), Estimation of surface-based duct parameters from surface clutter using a ray trace approach, *Radio Sci.*, *39*, RS6013, doi:10.1029/2003RS002930.

Barrios, A. E. (1994), A terrain parabolic equation model for propagation in the troposphere, *IEEE Trans. Antennas Propag.*, *42*(1), 90–98.

Barton, D. (1988), *Modern Radar System Analysis*, Artech House, Norwood, Mass.

Chan, H. C. (1990), Radar sea-clutter at low grazing angles, *IEE Proc.*, *137*(F-2), 102–112.

Dockery, G. D. (1990), Method of modelling sea surface clutter in complicated propagation environments, *IEE Proc.*, *137*(F–2), 73–79.

Gerstoft, P., L. T. Rogers, J. Krolik, and W. S. Hodgkiss (2003), Inversion for refractivity parameters from radar sea clutter, *Radio Sci.*, *38*(3), 8053, doi:10.1029/2002RS002640.

Gerstoft, P., W. S. Hodgkiss, L. T. Rogers, and M. Jablecki (2004), Probability distribution of low altitude propagation loss from radar sea-clutter data, *Radio Sci.*, *39*, RS6006, doi:10.1029/2004RS003077.

Hodur, R. M. (1996), The Naval Research Laboratory's Coupled Ocean/Atmosphere Mesoscale Prediction System (COAMPS), *Mon. Weather Rev.*, *125*(7), 1414–1430.

Jakeman, E., and P. N. Pusey (1976), A model for non-Rayleigh sea clutter, *IEEE Trans. Antennas Propag.*, *24*, 806–814.

Kay, S. M. (1993), *Fundamentals of Statistical Signal Processing*, vol. 1, *Estimation Theory*, Prentice-Hall, Upper Saddle River, N. J.

Konstanzer, G. C., J. Z. Gehman, M. H. Newkirk, and G. D. Dockery (2000), Calculation of surface incident field using TEMPER for land and sea clutter modeling, in *Meeting Proceedings on Low Grazing Angle Clutter: Its Characterization, Measurement and Application*, *NATO Res. Technol. Org. Rep., RTO-MP-60*.

Levy, M. (2000), *Parabolic Equation Methods for Electromagnetic Wave Propagation*, Inst. of Electr. Eng., London.

Long, M. W. (2000), *Radar Reflectivity of Land and Sea*, 3rd ed., Artech House, Norwood, Mass.

Lowry, A. R., C. Rocken, S. V. Sokolovskiy, and K. D. Anderson (2002), Vertical profiling of atmospheric refractivity from ground-based GPS, *Radio Sci.*, *37*(3), 1041, doi:10.1029/2000RS002565.

Ó Ruanaidh, J. J. K., and W. J. Fitzgerald (1996), *Numerical Bayesian Methods Applied to Signal Processing*, *Stat. Comput. Ser.*, Springer, New York.

Patterson, W. L. (2005), *User's Manual for Advanced Refractive Effect Prediction System*, 3.4 ed., Atmos. Propag. Branch, Space and Nav. Warfare Syst. Cent., San Diego, Calif.

Paulus, R. A. (1990), Evaporation duct effects on sea clutter, *IEEE Trans. Antennas Propag.*, *38*(11), 1765–1771.

Reilly, J. P., and G. D. Dockery (1990), Influence of evaporation ducts on radar sea return, *IEE Proc. Radar Signal Process.*, *137*(F–2), 80–88.

Rogers, L. T., C. P. Hattan, and J. K. Stapleton (2000), Estimating evaporation duct heights from radar sea echo, *Radio Sci.*, *35*(4), 955–966, doi:10.1029/1999RS002275.

Rogers, L. T., M. Jablecki, and P. Gerstoft (2005), Posterior distributions of a statistic of propagation loss inferred from radar sea clutter, *Radio Sci.*, *40*, RS6005, doi:10.1029/2004RS003112.

Rowland, J. R., and S. M. Babin (1987), Fine-scale measurements of microwave profiles with helicopter and low cost rocket probes, *Johns Hopkins APL Tech. Dig.*, *8*(4), 413–417.

Shnidman, D. A. (1999), Generalized radar clutter model, *IEEE Trans. Aerosp. Electron. Syst.*, *35*(3), 857–865.

Skolnik, M. I. (2001), *Introduction to Radar Systems*, 3rd ed., McGraw–Hill, New York.

Stahl, R. W., and D. A. Crippen (1994), *An Experimenters Guide to the NASA Atmospheric Sciences Research Facility*, Goddard Space Flight Cent., Wallops Flight Facil., Wallops Is., Va.

Tatarski, V. I., and M. Charnotskii (1998), On the behaviour of scattering from a rough surface for small grazing angles, *IEEE Trans. Antennas Propag.*, *46*(1), 67–72.

Thews, E. R. (1990), Timely prediction of low-altitude radar performance in operational environments using in situ atmospheric refractivity data, *IEE Proc.*, *137*(F–2), 89–94.

Vasudevan, S., R. Anderson, S. Kraut, P. Gerstoft, L. Rogers, and J. Krolik (2007), Recursive Bayesian electromagnetic refractivity estimation from radar sea clutter, *Radio Sci.*, *42*, RS2014, doi:10.1029/2005RS003423.

Ward, K. D. (1981), Compound representation of high resolution sea clutter, *Electron. Lett.*, *17*, 561–563.

Ward, K. D., R. J. A. Tough, and S. Watts (2006), *Sea Clutter: Scattering, the K Distribution and Radar Performance*, Inst. of Eng. and Technol., London.

Willitsford, A., and C. R. Philbrick (2005), Lidar description of the evaporative duct in ocean environments, *Proc. SPIE*, *5885*, 140–147.

Yardim, C., P. Gerstoft, and W. S. Hodgkiss (2006), Estimation of radio refractivity from radar clutter using Bayesian Monte Carlo analysis, *IEEE Trans. Antennas Propag.*, *54*(4), 1318–1327, doi:10.1109/TAP.2006.872673.

Yardim, C., P. Gerstoft, and W. S. Hodgkiss (2007), Statistical maritime radar duct estimation using a hybrid genetic algorithm–Markov chain Monte Carlo method, *Radio Sci.*, *42*, RS3014, doi:10.1029/2006RS003561.

Yardim, C., P. Gerstoft, and W. S. Hodgkiss (2008), Tracking refractivity from clutter using Kalman and particle filters, *IEEE Trans. Antennas Propag.*, *56*(4), 1058–1070, doi:10.1109/TAP.2008.919205.

P. Gerstoft, W. S. Hodgkiss, and C. Yardim, Marine Physical Laboratory, Scripps Institution of Oceanography, University of California, San Diego, La Jolla, CA 92037-0238, USA. (gerstoft@ucsd.edu; whodgkiss@ucsd.edu; cyardim@ucsd.edu)